

MODELING THE EFFECT OF MARINE SNOW FRAGMENTATION

BY *Euphausia pacifica* ON CARBON FLUX

HUMBOLDT STATE UNIVERSITY

By

Thè Thè Kyaw

A Thesis

Presented to

The Faculty of Humboldt State University

In Partial Fulfillment

Of the Requirements for the Degree

Master of Science

In Environmental Systems: Mathematical Modeling

August, 2008

MODELING THE EFFECT OF MARINE SNOW FRAGMENTATION

BY *Euphausia pacifica* ON CARBON FLUX

HUMBOLDT STATE UNIVERSITY

By

Thè Thè Kyaw

Approved by the Master's Thesis Committee:

Dr. Christopher Dugaw, Major Professor Date

Dr. Borbala Mazzag, Committee Member Date

Dr. Sarah Goldthwait, Committee Member Date

Dr. Christopher Dugaw, Graduate Coordinator Date

Chris A. Hopper, Interim Dean Date

Research, Graduate Studies & International Programs

ABSTRACT

MODELING THE EFFECT OF MARINE SNOW FRAGMENTATION

BY *Euphausia pacifica* ON CARBON FLUX

Thè Thè Kyaw

Marine snow aggregates are important components in the ocean carbon cycle because their sinking transports carbon from the surface layer of the ocean to the deep ocean where carbon can be sequestered for hundreds to thousands of years. The sedimentation rate of marine snow out of the mixed layer can be influenced by swimming euphausiids, *Euphausia pacifica*, because euphausiids are able to fragment a single aggregate into multiple smaller particles and potentially reduce carbon flux out of the ocean surface layer also known as the mixed layer. The interaction between rapidly sinking large particles and animal behavior has been recently discovered and there are not many studies on this process. We used a system of ordinary differential equations to develop a mathematical model that examines the change in the concentration and the total volume of aggregates with and without fragmentation by euphausiids and investigated how these changes influence marine snow sedimentation. Our results shows that through swimming behavior alone euphausiids are able to reduce carbon transport out of the ocean surface layer by approximately 30%. Fragmentation by euphausiids is an important process affecting marine snow sedimentation and the transport of carbon out of the mixed layer, and thus it has an impact on the global carbon cycle.

ACKNOWLEDGEMENTS

First and foremost, I would like to thank my thesis committee, Dr. Chris Dugaw, Dr. Sara Goldthwait, and Dr. Bori Mazzag, for their efforts and dedication to this project. I have learned a great deal from each of the committee members. It was a great honor to be their advisee and to study and teach at the Mathematics Department of Humboldt State University.

Dr. Chris Dugaw was a great help to me in the completion of this project and in achieving my goal of graduating in a timely manner. Many thanks to Dr. Dugaw for being an excellent advisor, providing me with the knowledge and skills, encouraging me, for his infinite patience, and for his sense of humor throughout this exciting and challenging journey. I greatly appreciate the time and energy he spent working on this project with me, especially in the summer. I can't thank him enough for his confidence in me and flexibility out of his busy schedule. If he had not been my advisor, I would not have had such a smooth journey while pursuing my dream. Dr. Dugaw is a fabulous teacher and a wonderful down-to-earth approachable man. I have had a wonderful time working with him.

I would like to thank Dr. Sarah Goldthwait for inspiring me to take on this project, for her availability to meet with me, and for all of the work she put into this project. Her enthusiasm, excellence in her field, comments about my writing, and wonderful personality were invaluable.

I would also like to thank Dr. Bori Mazzag for advising me in my first year at HSU, the time she spent on this project, her excellent editing skills, and her continued support even after I changed my thesis topic.

Huge thanks to my awesome roommate, Lourdes Triana, for sharing jokes with me, laughing with me, listening to me, helping me with a lot of other things, and most im-

portantly, watching movies with me after my long days of working. Special thanks to my crew: Daniele Rosa, for videotaping my thesis defense, listening to me practice my defense, and giving me honest comments on my writing and my ideas; Holly Perryman and Nicole Batenhorst for helping me release my stress by doing Yoga with me and for fun times; Liz Arnold, Emily Hobelmann, Iris Gray, and Erica Case for covering my classes when I needed and for their friendships. Many thanks to my best friend and cousin, Ma Thida Aye, for listening and letting me get my anxieties out. I would also like to thank all other colleagues as well as the other faculty who have taught me, supported me, and helped me in this journey.

At last but not the least, I would like to extend my gratitude, thanks, and love to my dear family in Myanmar (Burma), my sister's family in Japan, and my fiancé, Kan Tone, for supporting me both emotionally and financially throughout my study in the US. I am very lucky to have a pair of wonderful parents who love me dearly and who are always there for me. They taught me to be compassionate, to be strong, to be honest, and to be focused. I am a better person because of them. To them, I owe my M.S. Special thanks to my big sister, Ma Ma Ohn Mar, for listening to my complaints on the phone, for cheering me up when I am down, and for encouraging me to continue with this project. I am grateful to my fiancé for his love, his support, and his persistence in the past few years. Without their love, their wholehearted support, and their true belief in me, I would have gone nowhere.

TABLE OF CONTENTS

| | |
|---|-----|
| ABSTRACT | iii |
| ACKNOWLEDGEMENTS | iv |
| TABLE OF CONTENTS | vi |
| LIST OF FIGURES | vii |
| LIST OF TABLES | ix |
| INTRODUCTION | 1 |
| METHODS | 9 |
| Coagulation | 10 |
| Fragmentation | 16 |
| Sinking | 17 |
| Cell Division | 17 |
| Sixteen Ordinary Differential Equations | 18 |
| RESULTS | 22 |
| DISCUSSION | 30 |
| BIBLIOGRAPHY | 36 |
| APPENDIX | 39 |

LIST OF FIGURES

| Figure | Page |
|--------|---|
| 1 | Computing the proportion of resulting particles which go to the T_{ij}^{min} after the collision between particles of size classes i and j : σ_{ij} . The shaded regions represent the proportion of resulting particles that go to the T_{12}^{min} class after the collisions between particles of classes 1 and 2. (Note $T_{12}^{min} = T_{21}^{min} = 2$) 13 |
| 2 | Marine snow concentration and total volume by size class over time without fragmentation by euphausiids . Parameter values are: $\beta = 5 \times 10^{-4}$, $\mu = 0.75 \text{ d}^{-1}$, $z = 100 \text{ m}$, and $\alpha = 0.25$. Initial conditions are described in text. 23 |
| 3 | The concentration change in size classes 12, 13, and 14 for the first four days without fragmentation by euphausiids . Parameters are same as Figure 2. 24 |
| 4 | Marine snow concentration and total volume by size class over time with fragmentation by euphausiids . $\Phi = 1.410 \times 10^{-4} \text{ s}^{-1}$ and other parameters are same as Figure 2. 25 |
| 5 | The total volume of sinking aggregates with fragmentation by euphausiids versus without fragmentation by euphausiids . X axis is time ranging from day 0 to day 30. Y axis is the total volume of sinking aggregates of all size classes. Parameter values are: $\beta = 5 \times 10^{-4}$, $\mu = 0.75 \text{ d}^{-1}$, $z = 100 \text{ m}$, and $\alpha = 0.25$ 27 |
| 6 | The total particulate flux depending upon the different values of μ . X axis is the reproduction rate of size class 1 : μ range 0 – 1. Y axis is the total volume of sinking aggregates in all size classes. Parameter values are: $\beta = 5 \times 10^{-4}$, $z = 100 \text{ m}$, and $\alpha = 0.25$ 28 |
| 7 | The total particulate flux depending upon the different values of β . X axis is the contact rate: β range $1 \times 10^{-4} - 1 \times 10^{-3}$. Y axis is the total volume of sinking aggregates of all size classes. Parameter values are: $\mu = 0.75$, $z = 100 \text{ m}$, and $\alpha = 0.25$ 28 |

| | | |
|----|--|----|
| 8 | The total particulate flux depending upon the different values of α . X axis is the probability that particles stick together after contact: α range 0.1 – 1. Y axis is the total volume of sinking aggregates of all size classes. Parameter values are: $\mu = 0.75$, $z = 100$ m, and $\beta = 5 \times 10^{-4}$ | 29 |
| 9 | The total particulate flux depending upon the different values of z . X axis is the mixed layer depth: z range 50 m – 200 m. Y axis is the total volume of sinking aggregates of all size classes. Parameter values are: $\mu = 0.75$, $\alpha = 0.25$ m, and $\beta = 5 \times 10^{-4}$ | 29 |
| 10 | The difference between the two total volumes of particles (one with higher contact rate $\beta: 1 \times 10^{-3}$ and the other one with lower contact rate $\beta: 5 \times 10^{-4}$) that has sunk out of the mixed layer by size class. Other parameters are same as Figure 2. | 31 |
| 11 | The colormap for Figure 10. The blue shaded region represents when the total volume of sinking particles with large $\beta (1 \times 10^{-3})$ is greater than the total volume of sinking particles with small $\beta (5 \times 10^{-4})$ by size class. The green shaded regions represent when the difference is less than zero. Other parameters are same as Figure 2. | 32 |

LIST OF TABLES

| Table | | Page |
|-------|--|------|
| 1 | Ranges of Size Classes for Marine Snow Aggregates | 9 |
| 2 | Parameter and Variable Definitions for the System of Ordinary Differential Equations | 21 |

INTRODUCTION

Since the industrial revolution (around 1750), atmospheric carbon dioxide (CO_2) concentrations have been increasing rapidly due to human activities primarily burning of fossil fuels (coal, oil, and natural gas) and clearing forests (Falkowski et al., 2000; U.S. Climate Change Science Program, 2007). Global annual emissions of anthropogenic greenhouse gas (GHG) in 2004 was 49 gigatonnes (Gt) and about 57% of GHG emissions is due to fossil fuel use (Intergovernmental Panel on Climate Change, 2007). Before industrialization, CO_2 levels were between about 180 and 280 parts per million by volume (ppmv) (Falkowski et al., 2000). Now, atmospheric CO_2 concentration is approximately 380 ppmv which is higher than at any point in the past 650,000 years (Kolbert, 2006). Although CO_2 is important to Earth's energy balance and climate, excess carbon in the atmosphere increases the Earth's temperature (Sarmiento and Bender, 1994). A warming Earth can cause serious problems associated with global climate change such as a rise in the sea level, the disappearance of most remaining glaciers, more deadly droughts, air pollution, mass animal extinctions and increased fiercer hurricanes (Kolbert, 2006).

Some of the excess CO_2 is absorbed by the ocean and this mitigates global warming (Kolbert, 2006). In fact, nearly half of all the CO_2 that humans have emitted has been absorbed by the world's oceans since the beginning of the nineteenth century (Kolbert, 2006). Currently, there is considerable effort worldwide to understand the role of the oceans in the global carbon cycle (Sundquist and Visser, 2003). We review main aspects of the carbon cycle and the role the oceans play in it. The atmosphere and the uppermost ocean layer, called the mixed layer, exchange CO_2 continuously. First, CO_2 is built up in the atmosphere. As the ocean equilibrates with the atmosphere, CO_2 in the mixed layer increases. The build up of CO_2 in the atmosphere is slow since there is 50 times more CO_2 in the

ocean than in the atmosphere (Raven and Falkowski, 1999). Carbon dioxide absorbed by the ocean will eventually be released back into the air (Raven and Falkowski, 1999). Thus, the ocean is a major contributor to the carbon cycle since it is able to absorb and store carbon for decades to millions of years (Raven and Falkowski, 1999; Kolbert, 2006).

The two primary processes that transport carbon from the surface ocean to the ocean interior are the solubility pump and the biological pump (Falkowski et al., 2000). The solubility pump is a chemical process by which CO_2 dissolves in the ocean to form carbonic acid, bicarbonate and carbonate ions and is transported into the deep sea in dissolved form (Kolbert, 2006). The biological pump is a process in which CO_2 is incorporated into phytoplankton by photosynthesis and transported by various processes to the deeper cold-water, isolated from the atmosphere (Alldredge and Silver, 1988; Falkowski and Oliver, 2007). This biological pump keeps the atmospheric CO_2 level approximately 300 ppmv lower than it would be in the absence of phytoplankton, the primary photosynthetic organisms in the ocean (Falkowski et al., 2000; Falkowski and Oliver, 2007). Thus, the biological pump plays an important role in the ocean carbon cycle because it helps remove CO_2 from the oceans' surface and the oceans can, in turn, absorb more CO_2 from the atmosphere (Sarmiento and Bender, 1994). Therefore, we are interested in the ocean carbon cycle with a specific focus on the biological pump: the role of marine sinking particles in transporting carbon out of the sunlit zone or the euphotic zone (the well-lit surface layer of the ocean) and into the deep ocean where it can be sequestered for up to millions of years (Raven and Falkowski, 1999).

Phytoplankton are single-cell organisms which take up CO_2 through photosynthesis and are thus the primary component of the biological pump. The global phytoplankton production is 49 Gt per year (Martin et al., 1987). These microscopic organisms live at or near the ocean surface where there is sufficient sunlight for photosynthesis to occur.

Phytoplankton use solar energy to fix CO_2 and form glucose (Alldredge and Silver, 1988; Falkowski and Oliver, 2007). Dissolved CO_2 is taken up through photosynthesis by phytoplankton and particulate organic matter (POM) is formed. Due to their small size, single celled phytoplankton sink slowly. However, when phytoplankton become nutrient limited, their colonies often become more sticky, favoring aggregation (Passow, 2002). Then these living and non-living particles collide with other particles in the ocean and form large aggregates that can sink rapidly into the deep ocean.

Japanese researchers in the 1950s named these large sinking particles “marine snow” because they fall like snow in the deep water (Suzuki and Kato, 1953; Alldredge and Silver, 1988). Marine snow aggregates are usually defined as organic particles which are larger than 500 μm in diameter (Alldredge and Silver, 1988; Dilling and Alldredge, 2000). These aggregates have diverse origins because they are formed when small particles such as planktonic remains, fecal pellets, and detritus in the ocean collide and stick together (Alldredge and Silver, 1988). Thus, marine snow comes in a wide array of different shapes and has variable composition.

Marine snow plays an important role in the ocean carbon cycle because its sinking transports particulate organic carbon from the surface waters of the ocean to the deep sea or potentially the sea floor where carbon can be stored for hundreds to thousands of years (Fowler and Knauer, 1986; Alldredge and Silver, 1988). These large marine particles can sink up to 1000 m per day depending on size, shape and density (Fowler and Knauer, 1986). However, the concentration of sinking particles declines with increasing ocean depth (Fowler and Knauer, 1986; Martin et al., 1987). According to Falkowski and Oliver (2007) approximately 15% of the organic aggregates make it out of the surface ocean and only 0.1% of these sinking aggregates settle at the bottom of the seafloor. Due to their nutritional value, these falling aggregates are likely decomposed by bacteria or

consumed and respired by herbivores, releasing CO_2 to the water in the process, en route to the seafloor (Alldredge et al., 1987). Some of the released CO_2 is again taken up by phytoplankton and new POM is formed (Lampitt et al., 1993). Zooplankton, animal-like plankton, continue the transport of carbon by feeding on these organic particles and then defecating (Lampitt et al., 1993). The fecal matter can also aggregate with other algal cells, dead organisms, and other organic matter and form larger aggregates. When these carbon containing aggregates become large enough they can sink to the deep ocean or even to the sea floor (Alldredge and Silver, 1988; Jackson, 1990) where they may contribute to marine sediments and potentially sedimentary rocks (Raven and Falkowski, 1999; Falkowski and Oliver, 2007). However, due to the rapid regeneration in the mixed layer, majority of the CO_2 removed from upper 100 m in the form of marine snow will be again able to interact with the atmosphere on time scales of tens of years (Martin et al., 1987).

Particles in the ocean are brought together by three major mechanisms namely Brownian motion, fluid shear, and differential settlement (Pruppacher and Klett, 1980; Alldredge and Silver, 1988; Jackson, 1990). The first process, Brownian motion, is when random motions of particles cause some particles to collide (Pruppacher and Klett, 1980; Jackson, 1990). Mostly smaller particles are affected by this particular type of process and these have the greatest collision rate. The second process, fluid shear, occurs when fluid layers move at different velocities and/or different directions (Pruppacher and Klett, 1980; Jackson, 1990). Shear generated by small fluid-circulation can cause two particles to approach each other and touch. Most shear in the ocean is due to wind, and this process dominates the large particle aggregation. Finally, the last process, differential sedimentation, is when a rapidly sinking particle overtakes a more slowly sinking particle and then collides with it (Pruppacher and Klett, 1980; Jackson, 1990). These three processes coagulate organic particles and produce large, rapidly sinking marine snow aggregates.

Though there are several models that look at particle aggregation in marine systems, we will primarily focus on George Jackson's coagulation model because it is a mathematical model. Jackson (1990) developed a model based on a system of ordinary differential equations to analyze the dynamics of organic aggregates in the ocean. Jackson's model is a combination of kinetic coagulation theory and simple algal growth kinetics that explains the formation rate of aggregates and their sinking rate. Jackson (1990) describes, "coagulation theory refers to the rate of change in concentrations of a size class by adding the rates of all particle collisions which form aggregates of the size class, subtracting the rates of all collisions involving particles of the size which form larger particles, and subtracting the rate of particle loss to settling." Particle aggregation in his model is carried out by three major mechanisms: Brownian motion, fluid shear, and differential sedimentation. These three different processes for particle-particle contact are assumed to operate independently, allowing the total rate of formation of new particles to be expressed as the sum of the rates of the individual processes (Jackson, 1990). Jackson (1990) uses the number of single algal cells to describe his particles. His smallest size class contains particles with one cell, and every one higher size class has particles with one extra cell. In his formulation, the interaction rate of two particles is described by $C_i C_j \beta_{ij}$, where C_i and C_j represent the concentrations of particles containing i and j algal units and β_{ij} represents the coagulation kernel which is the sum of the terms describing the three coagulation processes. Not all collisions result in aggregation. Therefore, Jackson uses α to account for the probability that particles stick after contact. He describes the rate of the coagulation loss to settling as the abundance of particles that sinks through a unit area per unit time relative to the mixed layer depth. If z represents the mixed layer depth and w_i represents the particle settling rate which is a function of the particle radius r_i , then the rate of coagulation loss to settling is given by the flux, $w_i C_i$, divided by z . In his model, Jackson (1990) assumes that the con-

centration of particles with one algal cell, C_1 grows by cell division and higher size classes grow by the repetitive particle collisions. According to this coagulation model, particle size increases indefinitely.

Some studies have shown that particles can also be broken apart by a shear process (Spielman, 1978; Delichatsios and Probstein, 1974; Jackson, 1990), by feeding (Kioerboe, 2000) and swimming activities of zooplankton (Dilling and Alldredge, 2000; Goldthwait et al., 2004). Having a size-based disaggregation process places an effective upper size limit because the disaggregation process keeps particles from forming indeterminately large particles. Jackson (1990) also suggests that “incorporating particle break up in the model is more important than indefinite increases in particles size classes.” Although there are other biological or physical factors that can fragment large particles into numerous smaller particles, particle disaggregation is strongly influenced by the swimming activities of migrating euphausiids, for example *Euphausia pacifica* (Dilling and Alldredge, 2000; Goldthwait et al., 2004). The interaction between large particles and zooplankton swimming behavior has only recently been discovered and it has not been well studied (Dilling and Alldredge, 2000; Goldthwait et al., 2004). Therefore, our main goal is to modify Jackson’s model by adding the euphausiid particle fragmentation term and to examine the modified marine snow size spectrum.

Euphausiids, commonly known as krill, are vertically migrating crustaceans and *E. pacifica* is an abundant euphausiid off the coast of Northern California and in the California Current (Brinton, 1976). (Brinton, 1976). They generally spend the daylight hours at the ocean depths greater than 100 m and nighttime hours feeding on phytoplankton near the surface (Brinton, 1976). Krill are shrimp-like in appearance and part of the macrozooplankton larger than 2 mm in length. While swimming, a euphausiid creates a current around itself with an average radius of 6.7 mm that is capable of breaking large marine snow ag-

gregates into several smaller particles or “daughter aggregates” without loss of particulate organic carbon (Goldthwait et al., 2004). Smaller, slowly sinking particles tend to stay in the water column longer, potentially reducing the quantity of particles sedimenting out of the upper ocean (Dilling and Alldredge, 2000). Thus, euphausiids may have an important impact on the dynamics of marine snow sedimentation.

Dilling and Alldredge (2000) suggested that physical fragmentation by swimming euphausiids had a major impact on oceanic particle dynamics and might be a potential explanation for the decrease in POC flux with depth. Their field study showed that the abundance of euphausiids was positively correlated with aggregate concentration, but negatively correlated with average aggregate size in the Santa Barbara Channel. Although Dilling and Alldredge (2000) explained the interaction between swimming *E. pacifica* and large particles, they did not test it experimentally or extensively quantify this process.

Goldthwait et al. (2004) investigated the effect of swimming *E. pacifica* on particle size structure using aggregate sizes ranging from 0.5 to 14.7 mm in diameter and euphausiid sizes ranging from 13.6 to 24.3 mm. They found that 60% of aggregates were fragmented within a 6 mm radius of the euphausiid and most unfragmented particles were 0.5 – 0.6 mm in diameter. Each parent particle (particle prior to fragmentation) produces an average of 7.3 daughter particles and 60% of daughter particles are larger than 0.5 mm in diameter (Goldthwait et al., 2004). The number of daughter particles increases as the parent particle size increases; thus, krill has a major impact on the abundance and size distribution of large aggregates (Goldthwait et al., 2004). Due to physical fragmentation by swimming euphausiids, the abundance of small aggregates increases, but the overall marine snow mass decreases. This is of interest because the smaller aggregates will not sink as quickly as the large aggregates (Alldredge et al., 1990), potentially decreasing transport of carbon out of surface waters and weakening the efficiency of the so-called biological carbon pump

(Dilling and Alldredge, 2000; Goldthwait et al., 2004). Therefore, we primarily focus our attention on physical fragmentation of aggregates by swimming euphausiids, *E. pacifica*.

While particle coagulation has been modeled, there is a little known about the rates of marine snow fragmentation (Lampitt et al., 1993). Thus, we want to develop a mathematical model that investigates the variability in both the abundances and sizes of marine snow aggregates over time due to physical fragmentation by krill and how these changes influence carbon export. Our results will determine whether krill has a significant effect on marine snow sinking and storage of carbon beneath the upper mixed layer of the ocean.

METHODS

The process of collision and fragmentation of aggregates will be modeled using a system of ordinary differential equations. Our model is derived from George Jackson’s coagulation model (1990), but instead of using the number of single algal cells to describe particles, we use the total equivalent spherical volume of all the particles. In addition, our model incorporates aggregate fragmentation by *E. pacifica*. Since particles vary in volume, we create 16 different size classes to represent the particles. These size classes are classified according to ranges given in Table 1. Fragmentation experiments by Goldthwait et al. (2004) were performed on particles that range in size of 0.5 mm - 14.7 mm in diameter or 0.02 mm^3 - 218 mm^3 in equivalent spherical volume (ESV). Our size classes 4 to 15 represent their size classes.

Table 1: Ranges of Size Classes for Marine Snow Aggregates

| Size Class | Range (mm^3) | Size Class | Range (mm^3) |
|------------|--------------------------|------------|--------------------------------|
| class 1 | $0.000 < v_1 \leq 0.008$ | class 9 | $1.032 < v_9 \leq 2.065$ |
| class 2 | $0.008 < v_2 \leq 0.016$ | class 10 | $2.065 < v_{10} \leq 4.130$ |
| class 3 | $0.016 < v_3 \leq 0.032$ | class 11 | $4.130 < v_{11} \leq 8.260$ |
| class 4 | $0.032 < v_4 \leq 0.064$ | class 12 | $8.260 < v_{12} \leq 16.520$ |
| class 5 | $0.064 < v_5 \leq 0.129$ | class 13 | $16.520 < v_{13} \leq 33.040$ |
| class 6 | $0.129 < v_6 \leq 0.258$ | class 14 | $33.040 < v_{14} \leq 66.080$ |
| class 7 | $0.258 < v_7 \leq 0.516$ | class 15 | $66.080 < v_{15} \leq 132.160$ |
| class 8 | $0.516 < v_8 \leq 1.032$ | class 16 | $v_{16} > 132.16$ |

They also considered the case in which 0.5 mm particles are being fragmented by krill and produce smaller particles. To monitor these smaller particles, they used size class 1 ($0 < v_1 \leq 0.008$), class 2 ($0.008 < v_2 \leq 0.016$) and class 3 ($0.016 < v_3 \leq 0.032$). Goldthwait et al. (2004) found that the percentage of parents of particle sizes greater than 132.16 mm^3 ($\approx 6.3 \text{ mm}$ in diameter) was minimal ($< 0.5 \%$). Therefore we assume that any particle larger than 6.3 mm in diameter remains large even after being fragmented by

the krill and continues to sink fast. As a result, any particles larger than 135 mm^3 in volume will be considered to be in the largest size class (class 16). The total volume of particles in all size classes changes due to four basic processes: *coagulation*, *fragmentation*, *sinking*, and *cell division*.

Coagulation

In the first process, the interaction rate of two particles of sizes i and j is given by $C_i C_j \beta$, where β is the contact rate which is assumed to be constant; C_i and C_j are the concentrations of particles in size classes i and j , respectively. In Jackson's model, β was size dependent and ranged from 1×10^{-19} to 1×10^{-3} . Since our particle size classes are so much larger than Jackson's and his formulas predict unrealistically large contact rates for larger particles, we decided to make $\beta = 5 \times 10^{-4}$ constant in our model. C_i is approximated by dividing the total volume of particles in size class i , V_i , by the average volume of particles in size class i , \bar{v}_i . Since we assume the volume of individual particles is uniformly distributed over the range of volume, the average volume of particles in a size class, \bar{v} is actually the midpoint of the range and is constant. Because of the variable composition of particles, particles may not stick together every after contact (Pruppacher and Klett, 1978; Jackson, 1990). Therefore, the interaction rate $C_i C_j \beta$ is multiplied by the probability of sticking $\alpha = 0.25$ (Pruppacher and Klett, 1978; Jackson, 1990). This interpretation is applied to particles from all size classes.

After a collision, a newly formed particle either remains in the same class or move into a larger size class. Thus, the coagulation process is divided into two steps. The first step is coagulation loss, in which the volume of a particle is removed from the total volume of particles in its class. In the second step, coagulation gain, this volume is distributed to a

higher class and/or back into the class it came from. In the coagulation loss process, when two particles of a size class i and a size class j collide, the total volume of particles of size class i decreases by \bar{v}_i and the total volume of size class j decreases by \bar{v}_j . But, if particles of size class i collide with particles of the same size class, then the total volume of particles of size class i decreases by $2\bar{v}_i$ because two particles of the same size are lost. Like Jackson (1990), the Kronecker delta, δ_{ij} , is used to monitor the loss of two particles of the same size when they collide. The Kronecker delta δ_{ij} is equal to 1 if $i = j$, and 0 otherwise. For example, the coagulation loss of size class 1 due to particle collisions from its own size class can be described by $-2\alpha\bar{v}_1C_1C_1\beta$. If particles of size class 1 collide with particles of size class 2, then the coagulation loss of the size class 1 is given by $-\alpha\bar{v}_1C_1C_2\beta$. Thus, the total coagulation loss of size class i can be described in the following way:

$$\text{coagulation loss} = -\alpha\bar{v}_iC_i \sum_{j=1}^{15} (1 + \delta_{ij})C_j\beta. \quad (1)$$

Eq. 1 is applied to particles of all size classes except class 16 because we assume that size class 16 is the largest size class and particles from size class 16 sink fast enough so that other particles do not have a chance to collide with particles of size class 16. Therefore, the sum is only up to $j = 15$.

In the second step, coagulation gain, the total volume of particles from size class i increases by \bar{v}_i when the collision of two particles form a particle of size class i . When two particles collide, one from class i and one from class j with $i \geq j$, the resulting particle may fall in either class i or possibly class $i + 1$. Due to the particle size ranges, it is uncertain what the size class of a newly formed particle will be after contact. First of all, we checked what the size class of newly formed particle will be when two smallest particles, one from each size class or from the same size class, collide or when two largest particles collide.

Then, based on this observation we determined all possible coagulation of any two particles from size classes. We use T^{min} matrix to represent all possible transitions of newly formed particles resulting from colliding two smallest particles from size classes and T^{max} matrix to represent all possible transitions of newly formed particles resulting from colliding two largest particles from size classes. For example, the $(i, j)^{th}$ entry of T^{min} refers to the size class of the newly formed particle resulting from the collision of two smallest particles, one from size class i and one from size class j and is denoted by T_{ij}^{min} . We observe that the collision between two largest particles from size classes i and j with $i \geq j$ always produces a particle of size class $i + 1$ (Note $T_{ij}^{max} = i + 1$). The collision between two smallest particles from size classes i and j with $i \geq j$ produces a particle of size class i (Note $T_{ij}^{min} = i$). Thus, the resulting particles from any other particle collision must fall in either size class T_{ij}^{min} which is equal to i or size class T_{ij}^{max} which is equal to $i + 1$.

Due to the structure of the size classes, a continuous approach is used to compute the proportion that the resulting particle moves to size class T_{ij}^{min} which is equal to class i . Since we assume a uniform distribution of volumes of particles in a given class, the joint distribution of volumes of colliding classes i and j will be uniformly distributed over the rectangle $v_{min,i} < v_i < v_{max,i}$ by $v_{min,j} < v_j < v_{max,j}$, where v_i and v_j are the volumes of particles in size class i and j , respectively; $v_{max,i}$ and $v_{max,j}$ are the largest volumes of particles in size classes i and j , respectively; $v_{min,i}$ and $v_{min,j}$ are the smallest volumes of particles in size classes i and j , respectively. This is illustrated in Figure 1. Let B be the event that a particle of size class i collides with a particle of size class j and let A be the event that the resulting particle is of size class T_{ij}^{min} . Then the probability of colliding particles from size classes i and j is the area of the rectangle having a length of $v_{max,i} - v_{min,i}$ and a width of $v_{max,j} - v_{min,j}$ and is represented by $P(B)$. The proportion of resulting particles that go to size class T_{ij}^{min} after the collision between particles of size

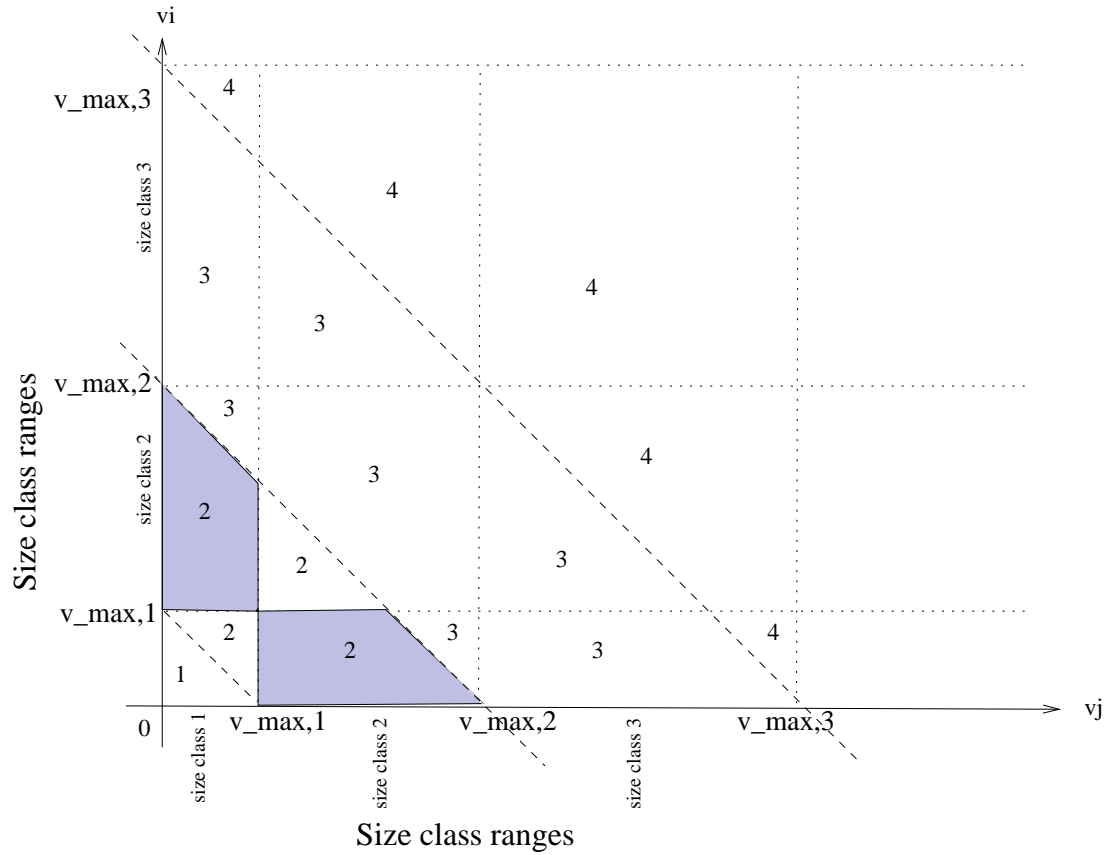


Figure 1: Computing the proportion of resulting particles which go to the T_{ij}^{min} after the collision between particles of size classes i and j : σ_{ij} . The shaded regions represent the proportion of resulting particles that go to the T_{12}^{min} class after the collisions between particles of classes 1 and 2. (Note $T_{12}^{min} = T_{21}^{min} = 2$)

classes i and j is the conditional probability that event A will occur, given that event B has occurred and is given by $\sigma_{ij} = P(A|B) = \frac{P(A \cap B)}{P(B)}$. If $v_i + v_j < \max(v_{max,i}, v_{max,j})$, the resulting particle will be of size class T_{ij}^{min} which is size class i if $i \geq j$; otherwise, it will be at size class T_{ij}^{max} . The function that indicates when a resulting particle will be in the T_{ij}^{min} class is given by

$$f(v_j, v_i) = \begin{cases} 1 & v_i < \max(v_{max,i}, v_{max,j}) - v_j \\ 0 & \text{otherwise} \end{cases}.$$

As shown in Figure 1, the function $f(v_i, v_j) = 1$ is the region below the line $v_i = \max(v_{max,i}, v_{max,j}) - v_j$. Then the probability that the resulting particle is of size class T_{ij}^{min} is obtained by integrating $f(v_i, v_j)$ over the intervals $v_{min,i} < v_i < v_{max,i}$ and $v_{min,j} < v_j < v_{max,j}$ and is represented by $P(A \cap B)$. Thus, the proportion of resulting particles that go to the T_{ij}^{min} class which is equal to size class i after the collision between particles of size classes i and j with $i \geq j$ is given by

$$\sigma_{ij} = P(A|B) = \frac{P(A \cap B)}{P(B)} = \frac{\int_{v_{min,i}}^{v_{max,i}} \int_{v_{min,j}}^{v_{max,j}} f(v_i, v_j) dv_j dv_i}{(v_{max,i} - v_{min,i})(v_{max,j} - v_{min,j})}. \quad (2)$$

Note that $(1 - \sigma_{ij})$ is the proportion of the resulting particles that go to the T_{ij}^{max} class which is size class $i + 1$. For example, the proportion of resulting particles that go to the T_{12}^{min} class (size class 2) after the collisions between particles of classes 1 and 2 is the shaded areas pictured in Figure 1 and the proportion of resulting particles that go to the T_{12}^{max} class (size class 3) is the triangular-shaped regions adjacent to the shaded regions. Since a particle of size class 1 hitting a particle of size 2 is considered the same as a particle of size class 2 hitting a particle of size class 1, only one of the shaded areas is counted and hence the probability is divided by 2. When two particles from size class 1 collide to form

a particle of size class 2, the total volume of size class 2 is assumed to be increased by $2\bar{v}_1$. The total volume of size class 2 can also be increased from other particle collisions. All possible collisions of particles that form size class 2 can be determined by using T^{min} and T^{max} matrices. According to T^{min} matrix (see Appendix), the collisions between two particles of size class 1 and size class 2 and between two particles of size class 2 form a particle of size class 2; based on T^{max} matrix, the collision between two particles of size class 1 form a particle of size class 2. Similarly, the collision which forms a particle of size class i can be determined using T^{min} and T^{max} . The total volume of size i is also assumed to be increased by $(\bar{v}_j + \bar{v}_k)$ if the collision between a particle of size j and a particle of size k forms a particle of size class i . The total coagulation gain in size class i is calculated by summing all the rates of collisions of particles which form particles of size class i and is given by:

$$0.5\alpha \sum_{jk:T_{jk}^{min}=i} \sigma_{jk}(\bar{v}_j + \bar{v}_k)C_j C_k \beta + 0.5\alpha \sum_{jk:T_{jk}^{max}=i} (1 - \sigma_{jk})(\bar{v}_j + \bar{v}_k)C_j C_k \beta, \quad (3)$$

where σ_{jk} is the proportion of collisions between particles of classes j and k that go to the T_{jk}^{min} class which is equal to class i ; $(1 - \sigma_{jk})$ is the proportion of collisions between particles of class j and k that go to the T_{jk}^{max} class which is also equal to class i . Note that j and k from T^{min} and j and k from T^{max} are not the same. In the similar way as in Jackson (1990), 0.5 is included to eliminate the double counting. This formulation is relevant to particles of all size classes except class 1 because class 1 is the smallest size class and there do not exist particles of sizes j and k smaller than size 1 which can form particles of size 1.

Fragmentation

The total volume of particles also changes in a size class due to fragmentation caused by krill. *E. pacifica* is capable of breaking particles into numerous, smaller particles by swimming. Depending on the type of particle and the size of krill, particles can be drawn in and fragmented from as far away as 37 mm from a swimming *E. pacifica* (Goldthwait et al., 2004). However, the majority of particles are fragmented within a 6 mm radius of the euphausiids and the average effective radius of fragmentation is $6.7 \text{ mm} \pm 3.5 \text{ mm}$ (Goldthwait et al., 2004). Thus, the effective radius $r = 6.7 \text{ mm}$ is used to calculate the fragmentation rate Φ in the model. When euphausiids swim in an aquatic system, they create cylindrical fluid stress around them. If a particle falls into this swimming path, it is fragmented. Thus, the volume per unit time effected by a single krill can be taken into account as the fragmentation rate Φ in our model. Assuming $r = 6.7 \text{ mm}$ and the swimming speed of a krill is about 100 mm per second (Torres and Childress, 1983), the volume of the fluid stress generated by a krill in a second fits with the formula for the volume of cylinder: $100\pi r^2 \approx 14102.61 \text{ mm}^3$. Typically, there are about 10 animals per m^3 (Mackie and Mills, 1983). Therefore, the fragmentation rate Φ used for our model was calculated using 10 krill per m^3 and hence $\Phi = 1.410 \times 10^{-4}$ per second.

The total volume of a size class i can be decreased when a particle from its size class is fragmented; it can also be increased when larger particles being fragmented by krill produce size class i particles. If a particle of size class i is fragmented by krill to produce a class j daughter particles, the total volume of size class i decreases by \bar{v}_j , where $j < i$. The rates of decline in the total volume of particles in size class i due to fragmentation is

represented by the following term:

$$\text{fragmentation loss} = -\Phi C_i D_i \sum_{j < i} \bar{v}_j \epsilon_{ji}, \quad (4)$$

where D_i is the number of daughter particles produced from parent particles of size i and ϵ_{ji} is a fraction of daughter particles of size j produced from parent particles of size i (Goldthwait et al., 2004). This formulation applies only to particles in size classes $i \geq 4$ because particles smaller than size class 4 are assumed not to be fragmented by euphausiids. The rates of growth in the total volume of particles in size class i resulting from fragmentation of larger particles can be derived as follows:

$$\text{fragmentation gain} = \bar{v}_i \sum_{j=i+1}^{15} \Phi C_j D_j \epsilon_{ij}. \quad (5)$$

Sinking

A particle is also considered to be lost if it sinks out of the mixed layer. The effect of sinking on total volume of particles in size class i is given by the ratio of the flux $v_i C_i w_i$ to the mixed layer depth of the ocean $z = 100$ m, where w_i is the settling rate (Jackson, 1990). The particle settling velocity is a function of the size of particles and is given by $w_i = 2\xi r_i^{1.17}$, where r_i is the radius of a particle in size class i and $\xi = 1.24 \text{cm}^{-0.17} \text{s}^{-1}$ is the curve-fit constant for w_i (Smayda, 1970; Jackson, 1989).

Cell Division

In the model, we assume that particles in size class 1 are actively growing phytoplankton cells that divide at a constant rate μ . The growth rate of total volume in class 1 due to cell

division is given by $\mu v_1 C_1$ (Jackson, 1990). Particles in any other size classes are assumed to be non-living and do not reproduce.

Sixteen Ordinary Differential Equations

Combining all these assumptions, the rate of change in the total volumes of particles in all size classes can be derived in the following way. Since we have 16 different size classes, our model consists of 16 ordinary differential equations. Each equation describes the rate of change in the total volume of an individual size class. These 16 size classes are divided into four groups depending on cell division, krill effect, and capability of coagulation. First consider the case of the total volume change in size class 1 ($< 0.01 \text{ mm}^3$), $\frac{dV_1}{dt}$. Particles in size class 1 can be formed by cell division and fragmentation of larger particles by krill. Particles in class 1 can be lost by colliding with each other to form larger particles, coagulation with other particles, and sinking out of the mixed layer. Thus, the total volume change in size class 1 obeys the following differential equation:

$$\frac{dV_1}{dt} = \mu \bar{v}_1 C_1 + \bar{v}_1 \Phi \sum_{j=4}^{15} C_j D_j \epsilon_{1j} - \alpha \bar{v}_1 C_1 \sum_{j=2}^{15} C_j \beta - (1 - \sigma_{11}) \alpha \bar{v}_1 C_1 C_1 \beta - \frac{\bar{v}_1 C_1 w_1}{z}. \quad (6)$$

Next we consider class 2 – 3 separately because particles of sizes 2 and 3 are assumed not to be fragmented by krill and not to be reproducing. Thus, the equation to represent the change of the total volume in size class i where $2 \leq i \leq 3$ is

$$\begin{aligned} \frac{dV_i}{dt} = & 0.5\alpha \sum_{jk: T_{jk}^{max}=i} (1 - \sigma_{jk})(\bar{v}_j + \bar{v}_k) C_j C_k \beta + 0.5\alpha \sum_{jk: T_{jk}^{min}=i} \sigma_{jk}(\bar{v}_j + \bar{v}_k) C_j C_k \beta \\ & + \bar{v}_i \Phi \sum_{j=4}^{15} C_j D_j \epsilon_{ij} - \alpha \bar{v}_i C_i \sum_{j=1}^{15} (1 + \delta_{ij}) \beta C_j - \frac{\bar{v}_i C_i w_i}{z}. \quad (7) \end{aligned}$$

The change in the total volume for size class i such that $4 \leq i \leq 15$ is similar to the case $2 \leq i \leq 3$, but we assume that particles in these size classes are being fragmented by the krill. So, the total volume change in these size classes fits with the following differential equation:

$$\begin{aligned} \frac{dV_i}{dt} = & 0.5\alpha \sum_{jk:T_{jk}^{max}=i} (1 - \sigma_{jk})(\bar{v}_j + \bar{v}_k)C_j C_k \beta + 0.5\alpha \sum_{jk:T_{jk}^{min}=i} \sigma_{jk}(\bar{v}_j + \bar{v}_k)C_j C_k \beta \\ & + \bar{v}_i \Phi \sum_{j=i+1}^{15} C_j D_j \epsilon_{ij} - \alpha \bar{v}_i C_i \sum_{j=1}^{15} (1 + \delta_{ij}) \beta C_j - \Phi C_i D_i \sum_{j<i} \bar{v}_j \epsilon_{ji} - \frac{\bar{v}_i C_i w_i}{z}. \end{aligned} \quad (8)$$

Finally, we consider the largest size class (class 16) separately because any particles from size class 16 that collide with any other particles or that fragment by krill always remain in the same size class. Therefore, the fragmentation loss term is not included in the model and the change in the total volume of size class 16 is represented by

$$\begin{aligned} \frac{dV_{16}}{dt} = & 0.5\alpha \sum_{jk:T_{jk}^{max}=16} (1 - \sigma_{jk})(\bar{v}_j + \bar{v}_k)C_j C_k \beta \\ & + 0.5\alpha \sum_{jk:T_{jk}^{min}=16} \sigma_{jk}(\bar{v}_j + \bar{v}_k)C_j C_k \beta - \frac{\bar{v}_{16} C_{16} w_{16}}{z}. \end{aligned} \quad (9)$$

We also keep track of the total volume of aggregates that has sunk out of the mixed layer by summing all the sinking terms. Our mathematical model is implemented in MATLAB. We obtain data such as the number daughter particles, D and a fraction of daughter particles remaining within the same size class, ϵ (see Appendix), from Sarah Goldthwait (Department of Oceanography, Humboldt State University) through personal communication. Goldthwait et al. (2004) collected these data while they investigated the interaction between marine snow and the physical fragmentation by *E. pacifica*. We use ordinary dif-

ferential equation solver 'ode45', medium order method, to solve a system of 16 ordinary differential equations. ode45 is based on Runge-Kutta method and is a function for the numerical solution of ordinary differential equations. As with any ordinary differential equation it is necessary to have an initial condition and thus the initial concentrations of particles are calculated using this formula $C_i = 1 \times 10^{-4} c_i^{-1}$, where c_i is the number of single algal cells in a particle of size class i . This formula is a variation of George Jackson's formula (1990) which is used to estimate the initial values for his coagulation model. The radius of the single algal cell, $r_1 = 0.001$ cm and the relationship between the radius of a particle in size class i , r_i and the number of single cells in that particle, c_i ($r_i = r_1 c_i^{0.44}$) are used to calculate c_i (Alldredge and Gotschalk, 1988; Jackson, 1990).

Table 2: Parameter and Variable Definitions for the System of Ordinary Differential Equations

| Parameter | Definition |
|-----------------|---|
| C_i | number of particles in size class i |
| V_i | total volume of particles in size class i |
| v_i | volume of a particle in size class i |
| \bar{v}_i | average volume of particles in size class i |
| $v_{max,i}$ | volume of the largest particle in size class i |
| $v_{min,i}$ | volume of the smallest particle in size class i |
| α | probability of particles that stick together after contact |
| μ | growth rate |
| β | collision rate |
| δ_{ij} | Kronecker delta |
| w_i | particles settling rate |
| ξ | curve-fit constant for w_i |
| z | mixed layer depth of the ocean |
| T_{ij}^{max} | size class of the newly formed particle resulting from the collision of two largest particles, one from size class i and one from size class j |
| T_{ij}^{min} | size class of the newly formed particle resulting from the collision of two smallest particles, one from size class i and one from size class j |
| A | event that the resulting particle is of size class T_{ij}^{min} |
| B | event that a particle of size class i collides with a particle of size class j |
| σ_{ij} | the proportion falling in the T_{ij}^{min} class after the collision between particles of sizes i, j |
| Φ | fragmentation rate of the krill |
| D_i | average number of daughters produced from a parent particle of size class i |
| ϵ_{ij} | fraction of daughters of size class i produced from a parent particle of size class j |

RESULTS

The model results are concentrations and total volumes for each size class, the total volume of sinking aggregates with and without fragmentation by krill, and the total particulate volume flux for different values of μ , β , α , and z with or without fragmentation by krill. In reality, the contact rates β and the probability that particles stick after contact (α) vary depending on the different size and the different types of marine snow aggregates. However, we assumed that the contact rate β for our particle size classes is not size dependent and the probability of sticking α is constant. Therefore, we tested our model for various values of β and α . Due to particle size ranges, we are not sure what proportion of particles in size class 1 represent actively growing phytoplankton cells that divide. Thus, our model is tested using various values for algal growth rate μ . As previously mentioned experimental measurements exist for all other parameters, so we choose not to test the sensitivity of the model to those. However, our analysis covers a broad range of possible parameter sets and captures the overall dynamics.

Without krill, no aggregate fragmentation occurs, therefore, the concentrations of size classes can only grow by coagulation process except in size class 1. Initially none of size classes increase significantly, but about two weeks later, the concentration of particles in size class 1, C_1 , starts increasing exponentially with time. The growth of C_1 slows down as it approaches its maximum, $0.085 \text{ particles cm}^{-3}$ (see Figure 2). At about 21 days C_1 reaches a critical concentration and then it decreases slightly until it achieves an equilibrium state where reproduction is balanced with coagulation and sinking. The new particles from size class 1 are fed into higher size classes by coagulation processes and rapidly sinking larger aggregates are produced.

As shown in Figure 2, the concentrations in size classes 2 to 5 grow a little from day

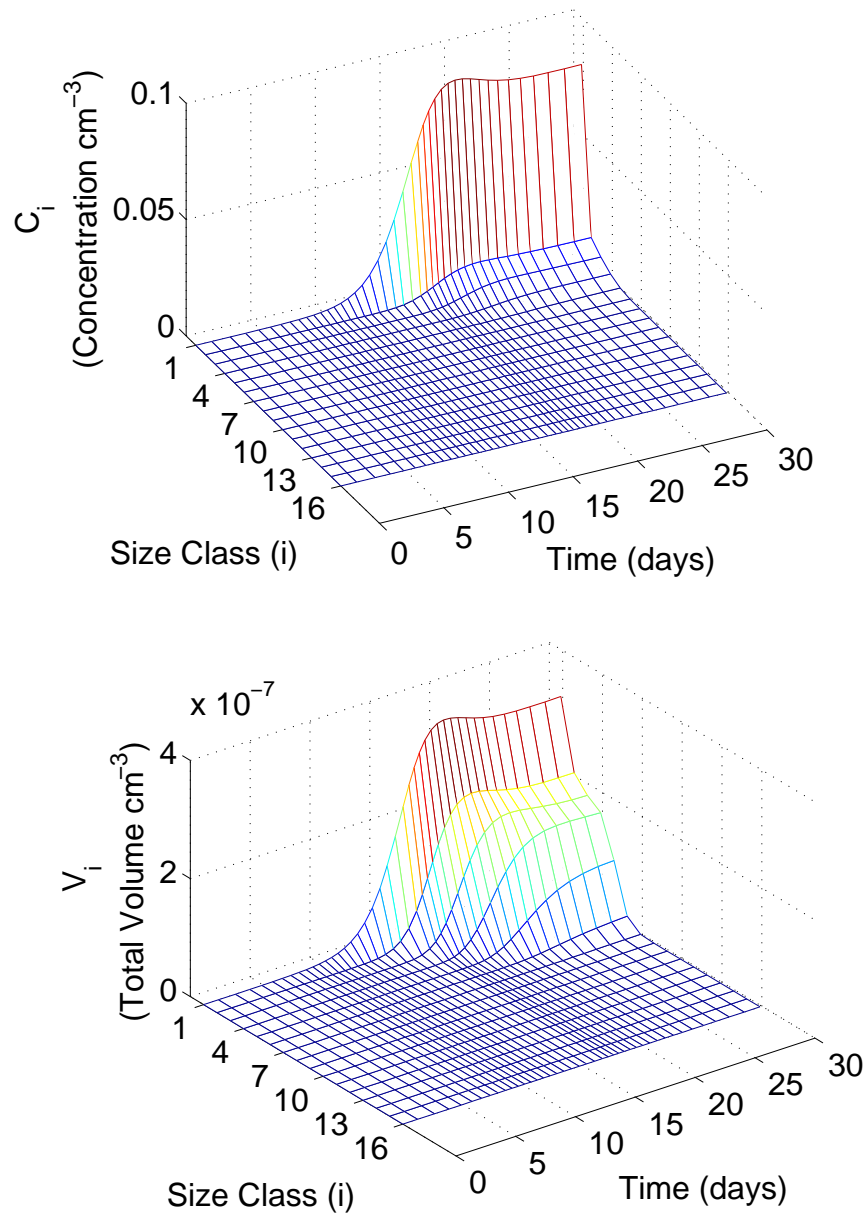


Figure 2: Marine snow concentration and total volume by size class over time **without fragmentation by euphausiids**. Parameter values are: $\beta = 5 \times 10^{-4}$, $\mu = 0.75 \text{ d}^{-1}$, $z = 100 \text{ m}$, and $\alpha = 0.25$. Initial conditions are described in text.

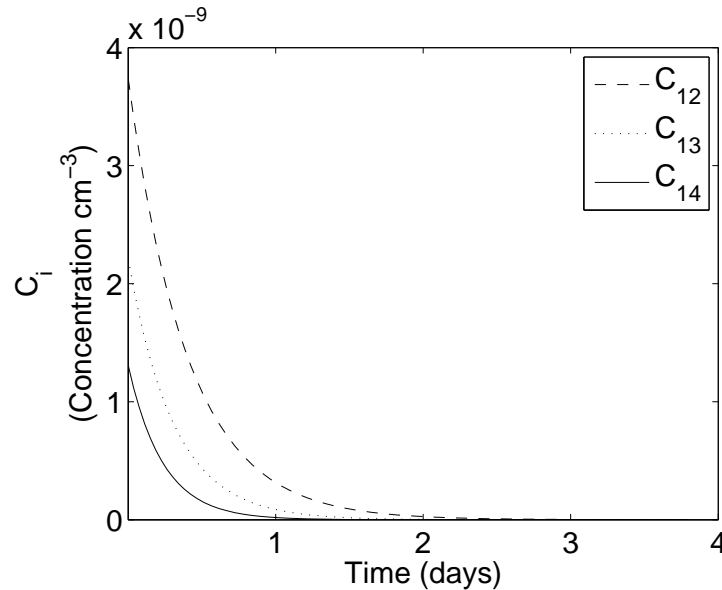


Figure 3: The concentration change in size classes 12, 13, and 14 for the first four days **without fragmentation by euphausiids**. Parameters are same as Figure 2.

10 until day 23 and then they start approaching the equilibrium distribution. Since particle concentrations in size classes 1 – 5 increase for about 13 days and the total volume is a product of the concentration and the average volume of particles, there is a noticeable increase in total volumes of these size classes at that time. The change in the particle concentrations of higher size classes 6 to 16 occurs fast as large aggregates sink out of the mixed layer more rapidly than they are formed. For instance, as shown in Figure 3, $C_{12} - C_{14}$ decrease rapidly and are approaching zero from day 0. At about 16 days, they grow back very slightly and one can barely notice this increase (see Figure 2). Thus, abundances as well as total volumes in higher size classes are approximately zero from day 1 on. We solved our model for various initial conditions and the results were qualitatively similar.

In the presence of krill, the results are similar to the results for the case without krill (see Figure 4), except there are more small particles as expected. Exponential increase of

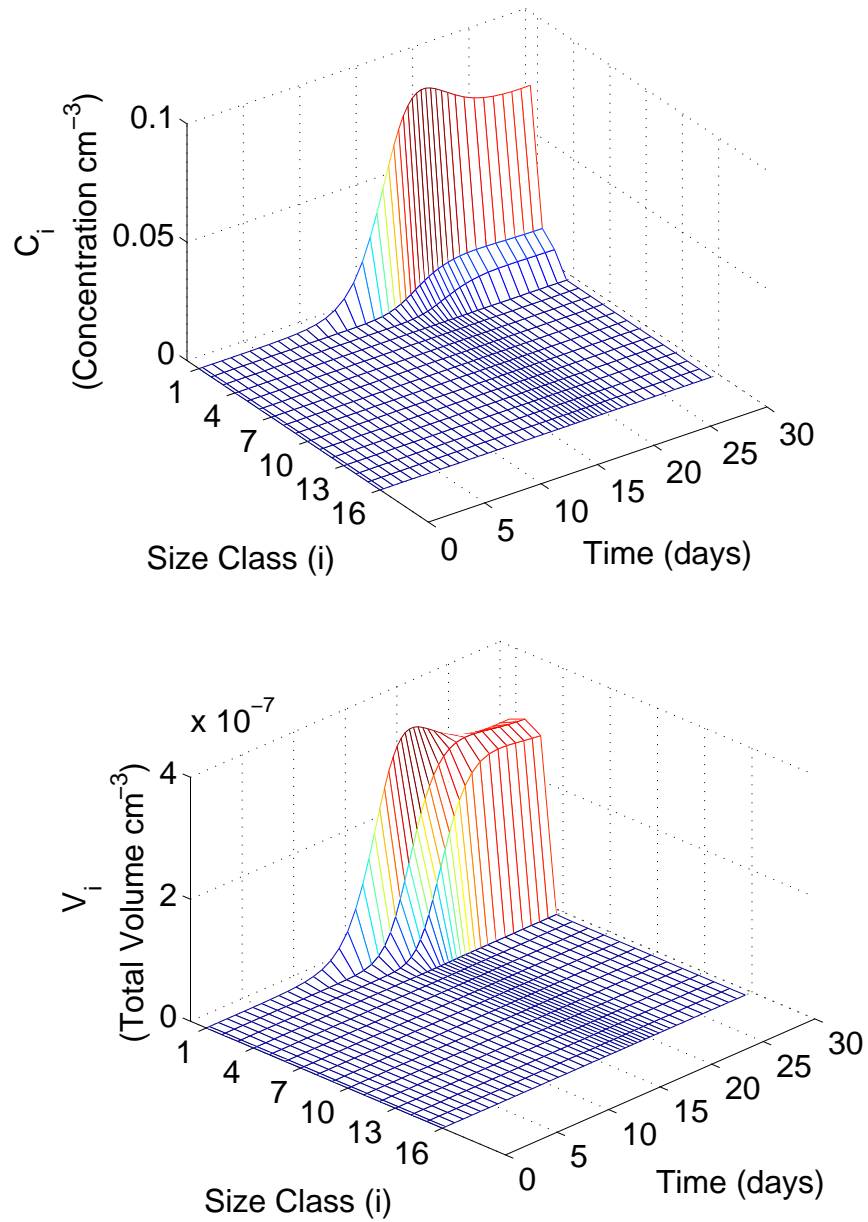


Figure 4: Marine snow concentration and total volume by size class over time **with fragmentation by euphausiids**. $\Phi = 1.410 \times 10^{-4} \text{s}^{-1}$ and other parameters are same as Figure 2.

C_1 slows and stops when it reaches a maximum concentration. C_2 and C_3 increase slightly at about day 12. Over the course of 8 days, they achieve the steady concentrations. In this case, particles in size classes 4 – 15 are fragmented by krill and produce smaller particles. Thus, the total volumes in size classes 1, 2, and 3 are significantly greater than the total volumes of size classes 4 – 15, which decrease quickly and are nearly zero as shown in Figure 4. The decrease in total volumes results in the decrease in concentration since the concentration is directly proportional to the total volume in our model. Thus, $C_4 - C_{15}$ also decline fast and are approximately zero due to fragmentation. Also notice that in the presence of krill the total volumes of size classes 2 and 3 are not only slightly greater than the total volume of size class 1, but also they are greater than the total volumes of size classes 2 and 3 without krill in the long run. With krill, V_2 and V_3 stop changing after arriving at $3 \times 10^{-7} \text{ cm}^{-3}$ and $2.8 \times 10^{-7} \text{ cm}^{-3}$, respectively; without krill, V_2 and V_3 become steady after reaching $2 \times 10^{-7} \text{ cm}^{-3}$ and $1.9 \times 10^{-7} \text{ cm}^{-3}$, respectively.

The particulate volume flux out of the mixed layer is affected by krill. Figure 5 shows that the total particulate organic matter that has sunk out of the mixed layer without krill is much higher than with krill after 20 days. For all parameter values we explored the system had reached equilibrium by 30 days. This justifies 30 days as a good time period to examine the difference between the particulate flux with krill and the particulate flux without krill. As shown in Figure 6, the total particulate volume flux increases with larger μ values when other parameters are fixed. So, more carbon is removed from the mixed layer when the growth rate of size class 1, μ , increases. The difference between the total particulate volume flux out of the mixed layer with krill and without krill is substantially larger when $\mu > 0.75$. Conversely, Figure 7 shows that the total particulate volume flux decreases with larger β values. In other words, less carbon is removed out of the mixed layer when β is bigger. The difference between the total particulate volume flux with

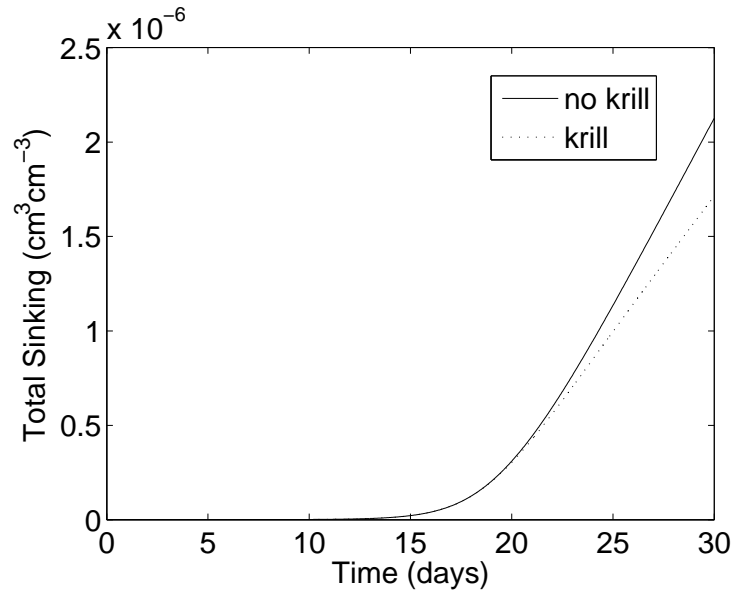


Figure 5: The total volume of sinking aggregates **with fragmentation by euphausiids** versus **without fragmentation by euphausiids**. X axis is time ranging from day 0 to day 30. Y axis is the total volume of sinking aggregates of all size classes. Parameter values are: $\beta = 5 \times 10^{-4}$, $\mu = 0.75 \text{ d}^{-1}$, $z = 100 \text{ m}$, and $\alpha = 0.25$.

krill and without krill does not vary significantly for β values ranging from 0.1×10^{-3} to 0.5×10^{-3} . However, after $\beta = 0.5 \times 10^{-3}$, the curves representing volume flux with krill and without krill start to become close. We notice that the result for increasing the probability of sticking α is very similar to the result for increasing β (see Figure 8). When α increases, the flux of the total volume of particles also decreases. Lastly, we also examine the change in the total volume flux by varying values of the mixed layer depth z since the mixed layer depth of the ocean is different from place to place. As the mixed layer depth z increases, the flux of the total volume of particles decreases slowly (see Figure 9). The decline in the total volume flux with krill is greater than without krill. Unlike large β , the change in the total volume flux of particle matter is steady, especially, without krill.

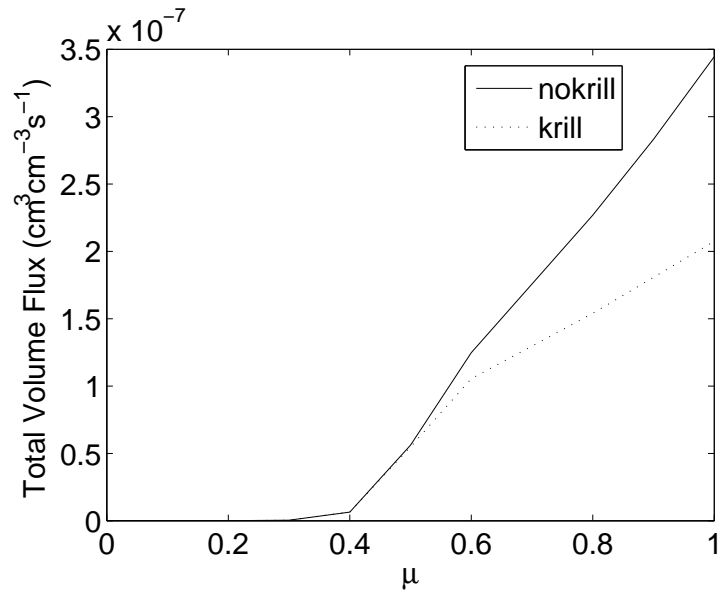


Figure 6: The total particulate flux depending upon the different values of μ . X axis is the reproduction rate of size class 1 : μ range 0 – 1. Y axis is the total volume of sinking aggregates in all size classes. Parameter values are: $\beta = 5 \times 10^{-4}$, $z = 100$ m, and $\alpha = 0.25$.

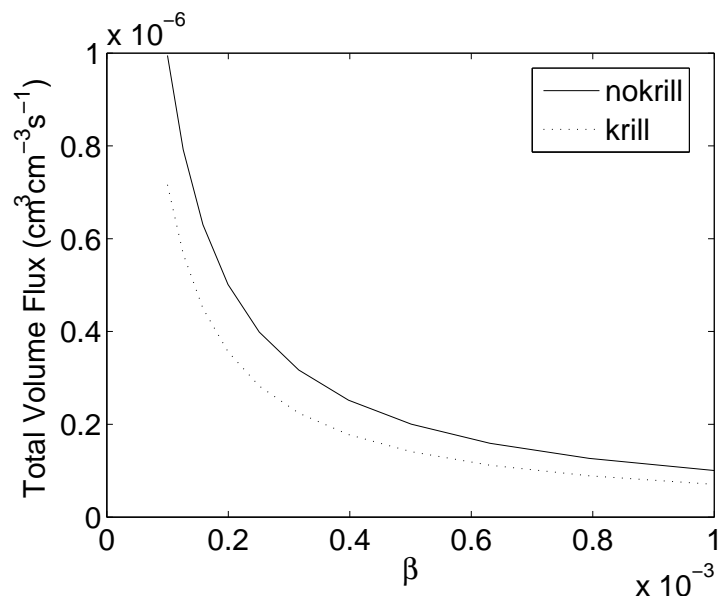


Figure 7: The total particulate flux depending upon the different values of β . X axis is the contact rate: β range $1 \times 10^{-4} - 1 \times 10^{-3}$. Y axis is the total volume of sinking aggregates of all size classes. Parameter values are: $\mu = 0.75$, $z = 100$ m, and $\alpha = 0.25$.

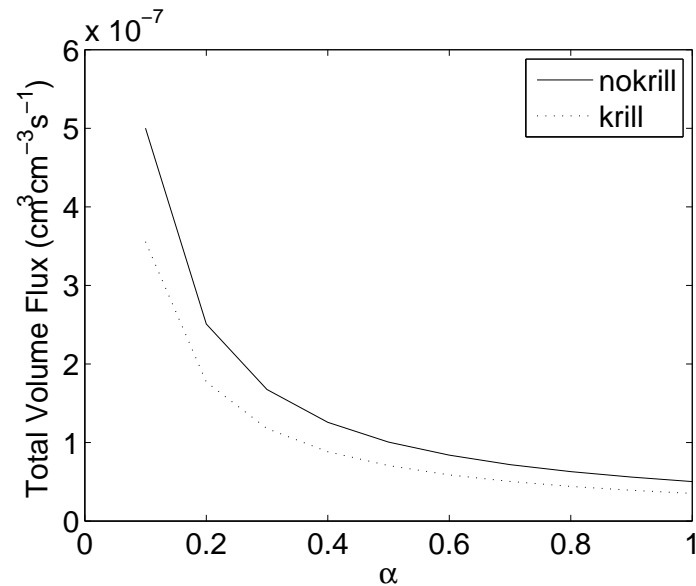


Figure 8: The total particulate flux depending upon the different values of α . X axis is the probability that particles stick together after contact: α range 0.1 – 1. Y axis is the total volume of sinking aggregates of all size classes. Parameter values are: $\mu = 0.75$, $z = 100$ m, and $\beta = 5 \times 10^{-4}$.

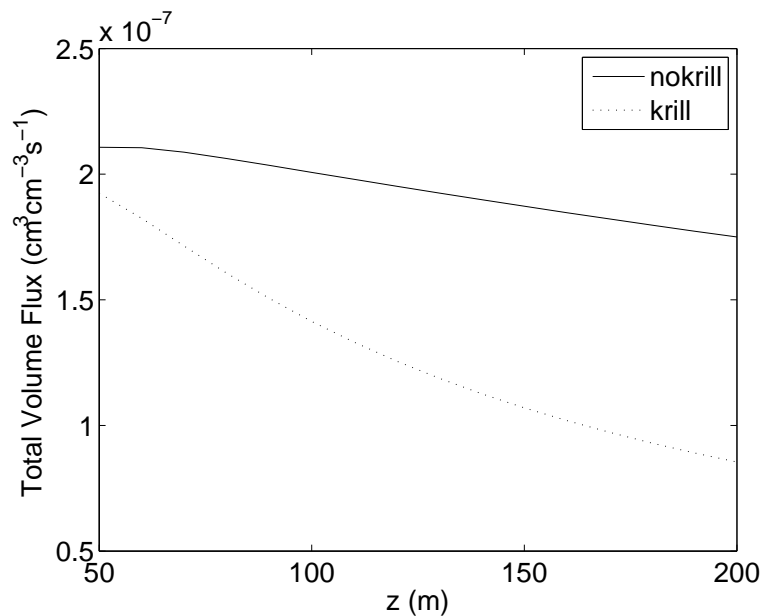


Figure 9: The total particulate flux depending upon the different values of z . X axis is the mixed layer depth: z range 50 m – 200 m. Y axis is the total volume of sinking aggregates of all size classes. Parameter values are: $\mu = 0.75$, $\alpha = 0.25$ m, and $\beta = 5 \times 10^{-4}$.

DISCUSSION

Through developing a marine snow fragmentation model by modifying Jackson's (1990) coagulation model and by using data obtained from Goldthwait et al. (2004), we were able to show that *E. pacifica* does indeed have an effect on the sinking rate of the particulate organic carbon and particle size distributions. In the presence of krill, there is increase in the total volume of particles in smaller size classes as particles in higher size classes are being fragmented to produce smaller, slower sinking particles. Thus, fragmentation by swimming krill increases the abundance of particles from size classes 1, 2, and 3 and decreases the abundance of large particles which are the major transporters of carbon out of the mixed layer and into the deep ocean (Fowler and Knauer, 1986; Alldredge and Silver, 1988). Consequently, the total amount of aggregates sinking declines with the presence of krill, implying that krill are inhibiting particulate flux, and thus carbon flux, out of the mixed layer. The decline in particulate flux leads to the decline in carbon flux because particulate organic matter contains 17 – 39% carbon by weight (Alldredge, 1998). The reduction in particulate flux due to fragmentation by krill is dependent on the algal growth rate, μ (Figure 6). There is about 30% reduction in the flux of particulate organic matter due to krill fragmentation when $\mu = 0.75$. This reduction percentage gets larger quickly as μ approaches 1.

The algal growth rate, μ , has a profound effect on the flux of particulate matter and larger values of μ boost the flux. Since μ represents the reproduction rate of size class 1 and particles in this class can form larger aggregates by colliding with any other particles, size class 1 is considered to be the primary source of the coagulation process. Hence, increasing μ leads to the formation of a greater number of large sinking aggregates. Thus, more carbon enters the deep ocean through sinking of these large aggregates when μ increases, but β is

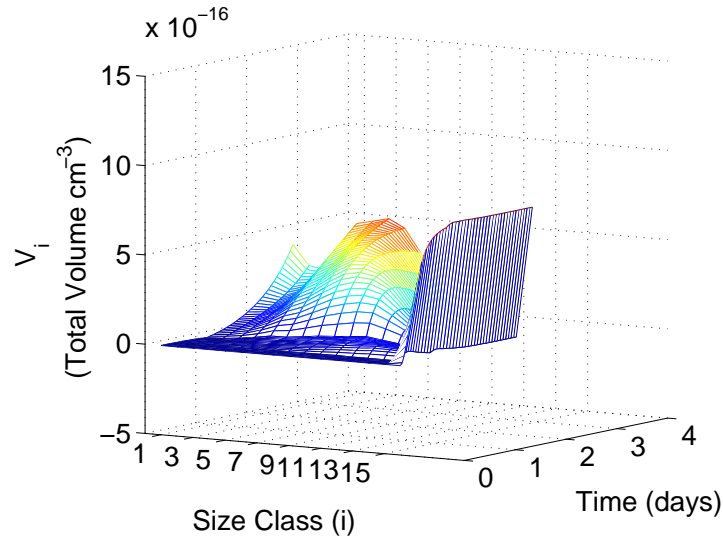


Figure 10: The difference between the two total volumes of particles (one with higher contact rate β : 1×10^{-3} and the other one with lower contact rate β : 5×10^{-4}) that has sunk out of the mixed layer by size class. Other parameters are same as Figure 2.

held constant. As a result, the carbon sinking rates increase rapidly and almost linearly with larger μ in the absence of krill. We expected that larger β would increase carbon flux as the higher contact rates would promote particle collisions which would, in turn, led to the formation of more large, rapidly sinking particles. However, Figure 7 disproves our anticipated results concerning the higher contact rates. Due to a particularly high contact rate, the coagulation process occurs faster and a large quantity of rapidly sinking, larger particles are formed. Quickly, these large particles sink out of the mixed layer and deplete the particle pool. Figure 10 evidently shows that more particles from size classes 5 – 16 are produced and sink out of the mixed layer with large β in the long run. The colormap (see Figure 11) specifically indicates which size class and what time the concentration of sinking aggregates with large β is greater than with small β . Eventually, mostly buoyant small particles remain. These small particles lose the chance to collide with large particles to form even larger particles. Therefore, less carbon in the form of marine snow sinks in the

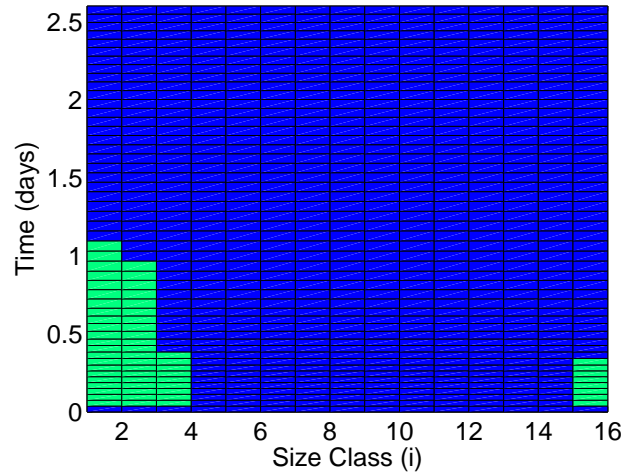


Figure 11: The colormap for Figure 10. The blue shaded region represents when the total volume of sinking particles with large β (1×10^{-3}) is greater than the total volume of sinking particles with small β (5×10^{-4}) by size class. The green shaded regions represent when the difference is less than zero. Other parameters are same as Figure 2.

long run. In other words, the total amount of carbon flux declines when the reproduction rate in class 1 cannot keep up with the coagulation process due to an unrealistically large contact rate. Similar results are found for increasing α (see Figure 8). Mathematically, increasing α is the same as increasing β because α and β are included in the same term of all of the equations. From the biological point of view, larger α implies that the particles are more likely to stick together after contact. Thus, larger particles are more likely to be formed and sink out of the mixed layer rapidly. This leads to the depletion of the particle pool and potentially reduces carbon flux. We also observed that increasing the mixed layer depth z led to the potential reduction in carbon flux. It makes sense because the sinking term $\frac{\bar{v}_i C_i w_i}{z}$ gets smaller as z gets larger which implies less concentration of sinking particles. In the presence of krill, the flux of the total volume of particles decreases faster (see Figure 9) since there are more buoyant small particles due to fragmentation and it takes longer for these small particles to sink out of the deeper mixed layer depth.

Like Jackson (1990), we attempted to use size-dependent β when we formulated our mathematical model, but it produced unrealistic results. The size dependent β values can be calculated using the simple coagulation kernel formula which is the sum of the rates of three major aggregation processes (Pruppacher and Klett, 1978; Jackson, 1990). For the range of particle sizes considered by Jackson (1990), the largest β was approximately 1.3×10^{-3} , whereas for our particle sizes β was as large as 0.574. This contact rate for big particles are unrealistically large because it does not make sense that bigger particles are more likely to collide with other particles and form indefinitely large particles. In natural systems, particle size does not increase indeterminately Jackson (1990) because when particles become too large, they become fragile and easy to break up. In fact, the particles larger than 0.7 mm in diameter break up by the same shear that brings particles together (Delichatsios and Probst, 1974; Spielman, 1978; Jackson, 1990). We used a different shear formula for particles larger in diameter (≥ 0.7 mm) (Hill et al., 1992), but the results were still impractical. This provides further justification for the choice of β in our model. We suggest that more research into particle dynamic of large particles in natural settings should be done.

The potential improvement for our model is to use a continuous function of total volumes as a function of size. Since we use a discrete approach to examine the formation and the fragmentation of marine snow, not all particles of consecutive sizes are tracked. For instance, the abundance of particles in size of 0.5 mm in diameter should be tracked separately from particles in size of 0.6 mm in diameter although they belong to the same size class because the particle sinking rate depends on its size. In addition, the continuous method allows a different assumption about the distribution of volumes of particles instead of the uniform distribution. However, such a model may be too complex to analyze effectively.

We observed that the concentrations and the total volumes of particles in higher size classes decreased quickly as large particles sank out of the mixed layer rapidly. This may be a result of overestimating sinking rates for large particles. Some studies observed that the residence time of some large marine snow in the surface layer is longer than small aggregates depending on the density of an aggregate and its surrounding environmental conditions (Asper, 1987; Riebesell, 1992). Asper (1987) observed that marine snow in diameter 4 – 5 mm had average sinking rates of 1 m per day. In contrast, our sinking rate is 324 m per day which is obtained by using the formula $w_i = 2\xi r_i^{1.17}$, where r_i is the radius of a particle in size class i and $\xi = 1.24\text{cm}^{-0.17}\text{s}^{-1}$ Jackson (1990). Our sinking rates for large particles tend to be much higher than those estimated. However, Fowler and Knauer (1986) observed that marine snow can sink up to 1000 m per day. Alldredge and Gotschalk (1988) stated that they never observed rates as low as the 1 m per day. In addition, Riebesell (1992) suggested that buoyancy of the large marine snow flocs was related to gas bubble formation within the flocs. Due to the fragile nature of the aggregates, it is particularly difficult to determine their sinking rates accurately (Asper, 1987) and the relationship between settling velocity and aggregate properties such as size, mass, and density are not known (Alldredge and Gotschalk, 1988).

Studying ocean particle dynamics helps us better understand the biological pump of the ocean carbon cycle and how the ocean plays a critical role in regulating Earth's temperature by absorbing much of the atmospheric CO_2 . Oceanic carbon stores and the events that lessen carbon storage have become increasingly important in understanding changes in the earth's climate. Though there may be other mechanisms that inhibit carbon sinking, we have focused our efforts on the euphausiid swimming behavior. All euphausiids have similar morphology; that means that likely all euphausiids can fragment marine snow into smaller particles (Dilling and Alldredge, 2000). Euphausiids are distributed worldwide, but

are most abundant in eutrophic (high nutrient) upwelling regions (Brinton, 1976). However, this is also where particulate flux and marine snow concentration are elevated. Therefore, we expect fragmentation to potentially be an important process regulating CO_2 sequestration in these productive regions. Our results indicate that the fragmentation of marine snow aggregates by swimming euphausiids weakens the strength of the biological pump and reduces the overall flux of particulate carbon. Ultimately, fragmentation by euphausiids has a large effect on particle dynamics and marine snow sedimentation, and thus, this process alters carbon flux.

BIBLIOGRAPHY

- Allredge, A. 1998. The carbon, nitrogen and mass content of marine snow as a function of aggregate size. *Deep-Sea Research Part I*, **45**:529–541.
- Allredge, A. L. and C. Gotschalk. 1988. In situ settling behavior of marine snow. *Limnology Oceanography*, **33**(3):339–351.
- Allredge, A. L., C. C. Gotschalk, and S. MacIntyre. 1987. Evidence for sustained residence of macrocrustacean fecal pellets in surface waters off Southern California. *Deep-Sea Research*, **34**(9):1641–1652.
- Allredge, A. L., T. C. Granata, C. C. Gotschalk, and T. D. Dickey. 1990. The physical strength of marine snow and its implications for particle disaggregation in the ocean. *Limnology Oceanography*, **35**(14):1415–1428.
- Allredge, A. L. and M. W. Silver. 1988. Characteristics, dynamics and significance of marine snow. *Progress in Oceanography*, **20**:41–82.
- Asper, V. L. 1987. Measuring the flux and sinking speed of marine snow aggregates. *Deep Sea Research Part I: Oceanographic Research*, **34**(1):1–17.
- Brinton, E. 1976. Population biology of *Euphausia pacifica* off Southern California. *Fishery Bulletin*, **74**(4):733–762.
- Delichatsios, M. A. and R. F. Probstein. 1974. Coagulation in turbulent flow-theory and experiment. *Journal of Colloid and Interface Science*, **51**(3):394–405.
- Dilling, L. and A. L. Allredge. 2000. Fragmentation of marine snow by swimming macrozooplankton: A new process impacting carbon cycling in the sea. *Deep-Sea Research Part I*, **47**(7):1227–1245.
- Falkowski, P., R. J. Scholes, E. Boyle, J. Canadell, D. Canfield, J. Elser, N. Gruber, K. Hibbard, P. Hogberg, S. Linder, et al. 2000. The global carbon cycle: a test of our knowledge of earth as a system. *Science*, **290**(5490):291–296.
- Falkowski, P. G. and M. J. Oliver. 2007. Mix and match: how climate selects phytoplankton. *Nature Reviews Microbiology*, **5**:813–819.
- Fowler, S. W. and G. A. Knauer. 1986. Role of large particles in the transport of elements and organic compounds through the oceanic water column. *Progress in Oceanography*, **16**(3):147–194.
- Goldthwait, S., J. Yen, J. Brown, and A. Allredge. 2004. Quantification of marine snow fragmentation by swimming euphausiids. *Limnology and Oceanography*, **49**(4):940–952.

- Hill, P. S., A. R. M. Nowell, and P. A. Jumars. 1992. Encounter rate by turbulent shear of particles similar in diameter to the Kolmogorov scale. *Journal of Marine Research*, **50**(4):643–668.
- Intergovernmental Panel on Climate Change. 2007. Climate change 2007: synthesis report. summary for policymakers. Tech. rep. URL <http://www.ipcc.ch/ipccreports/ar4-syr.htm>.
- Jackson, G. A. 1989. Simulation of bacterial attraction and adhesion to falling particles in an aquatic environment. *Limnology and Oceanography*, **34**:514–530.
- Jackson, G. A. 1990. A model of the formation of marine algal flocs by physical coagulation processes. *Deep-Sea Research*, **37**(8):1197–1211.
- Kioerboe, T. 2000. Colonization of marine snow aggregates by invertebrate zooplankton: Abundance, scaling, and possible role. *Limnology and Oceanography*, **45**(2):479–484.
- Kolbert, E. 2006. The darkening sea: what carbon emissions are doing to the ocean. *The New Yorker*, **20**.
- Lampitt, R. S., W. R. Hillier, and P. G. Challenor. 1993. Seasonal and diel variation in the open ocean concentration of marine snow aggregates. *Nature*, **362**(6422):737–739.
- Mackie, G. O. and C. E. Mills. 1983. Use of the Pisces IV submersible for zooplankton studies in coastal waters of British Columbia. *Canadian Journal of Fisheries and Aquatic Sciences*, **40**(6):763–776.
- Martin, J. H., G. A. Knauer, D. M. Karl, and W. W. Broenkow. 1987. VERTEX: Carbon cycling in the northeast Pacific. *Deep-Sea Research*, **34**(2):267–285.
- Passow, U. 2002. Transparent exopolymer particles (TEP) in aquatic environments. *Progress in Oceanography*, **55**:287–333.
- Pruppacher, H. R. and J. D. Klett. 1978. *Microphysics of clouds and precipitation*. D. Riedel Pub.
- Pruppacher, H. R. and J. D. Klett. 1980. *Microphysics of clouds and precipitation*. Riedel, Boston.
- Raven, J. A. and P. G. Falkowski. 1999. Oceanic sinks for atmospheric CO₂. *Plant, Cell and Environment*, **22**:741–755.
- Riebesell, U. 1992. The formation of large marine snow and its sustained residence in surface waters. *Limnology and Oceanography*, **37**(1):63–76.

- Sarmiento, J. L. and M. Bender. 1994. Carbon biogeochemistry and climate change. *Photosynthesis Research*, **39**(3):209–234.
- Smayda, T. R. 1970. The suspension and sinking of phytoplankton in the sea. *Oceanography and Marine Biology, Annual Review*, **8**:353–414.
- Spielman, L. A. 1978. Hydrodynamic aspects of flocculation. In K. J. Ives, ed., *The scientific basis of flocculation*. Sijthoff and Noordhoff, Alphen ann den Rijn, The Netherlands.
- Sundquist, E. T. and K. Visser. 2003. The geological history of the carbon cycle. *Treatise on Geochemistry, Biogeochemistry*, **8**:425–472.
- Suzuki, N. and K. Kato. 1953. Studies on suspended materials. Marine snow in the sea. Part I: sources of marine snow. *Bulletin of the Faculty of Fisheries, Hokkaido University*, **4**(2):132–137.
- Torres, J. J. and J. J. Childress. 1983. Relationship of oxygen consumption to swimming speed in *Euphausia pacifica*. I. Effects of temperature and pressure. *Marine Biology*, **74**:79–86.
- U.S. Climate Change Science Program. 2007. The first state of the carbon cycle report (SOCCR): the North American carbon budget and implications for the global carbon cycle. Tech. rep. URL <http://www.climatescience.gov/Library/sap/sap2-2/>.

APPENDIX

The following matrices are used in our model:

The transition matrix T^{min} provides all possible transitions of two smallest particles after contact. For example, the $(2, 3)^{th}$ entry of T^{min} represents the size class of the newly formed particle (in this case, which is 3) resulting from the collision of two smallest particles, one from size class 2 and one from size class 3

$T^{min} =$

| | | | | | | | | | | | | | | | | |
|----|----|----|----|----|----|----|----|----|----|----|----|----|----|----|----|----|
| 1 | 2 | 3 | 4 | 5 | 6 | 7 | 8 | 9 | 10 | 11 | 12 | 13 | 14 | 15 | 16 | |
| 2 | 2 | 3 | 4 | 5 | 6 | 7 | 8 | 9 | 10 | 11 | 12 | 13 | 14 | 15 | 16 | |
| 3 | 3 | 3 | 4 | 5 | 6 | 7 | 8 | 9 | 10 | 11 | 12 | 13 | 14 | 15 | 16 | |
| 4 | 4 | 4 | 4 | 5 | 6 | 7 | 8 | 9 | 10 | 11 | 12 | 13 | 14 | 15 | 16 | |
| 5 | 5 | 5 | 5 | 5 | 6 | 7 | 8 | 9 | 10 | 11 | 12 | 13 | 14 | 15 | 16 | |
| 6 | 6 | 6 | 6 | 6 | 6 | 7 | 8 | 9 | 10 | 11 | 12 | 13 | 14 | 15 | 16 | |
| 7 | 7 | 7 | 7 | 7 | 7 | 7 | 8 | 9 | 10 | 11 | 12 | 13 | 14 | 15 | 16 | |
| 8 | 8 | 8 | 8 | 8 | 8 | 8 | 8 | 9 | 10 | 11 | 12 | 13 | 14 | 15 | 16 | |
| 9 | 9 | 9 | 9 | 9 | 9 | 9 | 9 | 9 | 10 | 11 | 12 | 13 | 14 | 15 | 16 | |
| 10 | 10 | 10 | 10 | 10 | 10 | 10 | 10 | 10 | 10 | 11 | 12 | 13 | 14 | 15 | 16 | |
| 11 | 11 | 11 | 11 | 11 | 11 | 11 | 11 | 11 | 11 | 11 | 12 | 13 | 14 | 15 | 16 | |
| 12 | 12 | 12 | 12 | 12 | 12 | 12 | 12 | 12 | 12 | 12 | 12 | 13 | 14 | 15 | 16 | |
| 13 | 13 | 13 | 13 | 13 | 13 | 13 | 13 | 13 | 13 | 13 | 13 | 13 | 13 | 14 | 15 | 16 |
| 14 | 14 | 14 | 14 | 14 | 14 | 14 | 14 | 14 | 14 | 14 | 14 | 14 | 14 | 14 | 15 | 16 |
| 15 | 15 | 15 | 15 | 15 | 15 | 15 | 15 | 15 | 15 | 15 | 15 | 15 | 15 | 15 | 15 | 16 |
| 16 | 16 | 16 | 16 | 16 | 16 | 16 | 16 | 16 | 16 | 16 | 16 | 16 | 16 | 16 | 16 | 16 |

The transition matrix T^{max} provides all possible transitions of two largest particles after contact. For example, the size class of the newly formed particle resulting from the collision of two largest particles, one from size class 2 and one from size class 3, is given at the $(2, 3)^{th}$ entry of T^{max} .

$T^{max} =$

| | | | | | | | | | | | | | | | |
|----|----|----|----|----|----|----|----|----|----|----|----|----|----|----|----|
| 2 | 3 | 4 | 5 | 6 | 7 | 8 | 9 | 10 | 11 | 12 | 13 | 14 | 15 | 16 | 16 |
| 3 | 3 | 4 | 5 | 6 | 7 | 8 | 9 | 10 | 11 | 12 | 13 | 14 | 15 | 16 | 16 |
| 4 | 4 | 4 | 5 | 6 | 7 | 8 | 9 | 10 | 11 | 12 | 13 | 14 | 15 | 16 | 16 |
| 5 | 5 | 5 | 5 | 6 | 7 | 8 | 9 | 10 | 11 | 12 | 13 | 14 | 15 | 16 | 16 |
| 6 | 6 | 6 | 6 | 6 | 7 | 8 | 9 | 10 | 11 | 12 | 13 | 14 | 15 | 16 | 16 |
| 7 | 7 | 7 | 7 | 7 | 7 | 8 | 9 | 10 | 11 | 12 | 13 | 14 | 15 | 16 | 16 |
| 8 | 8 | 8 | 8 | 8 | 8 | 8 | 9 | 10 | 11 | 12 | 13 | 14 | 15 | 16 | 16 |
| 9 | 9 | 9 | 9 | 9 | 9 | 9 | 9 | 10 | 11 | 12 | 13 | 14 | 15 | 16 | 16 |
| 10 | 10 | 10 | 10 | 10 | 10 | 10 | 10 | 10 | 11 | 12 | 13 | 14 | 15 | 16 | 16 |
| 11 | 11 | 11 | 11 | 11 | 11 | 11 | 11 | 11 | 11 | 12 | 13 | 14 | 15 | 16 | 16 |
| 12 | 12 | 12 | 12 | 12 | 12 | 12 | 12 | 12 | 12 | 12 | 13 | 14 | 15 | 16 | 16 |
| 13 | 13 | 13 | 13 | 13 | 13 | 13 | 13 | 13 | 13 | 13 | 13 | 14 | 15 | 16 | 16 |
| 14 | 14 | 14 | 14 | 14 | 14 | 14 | 14 | 14 | 14 | 14 | 14 | 14 | 15 | 16 | 16 |
| 15 | 15 | 15 | 15 | 15 | 15 | 15 | 15 | 15 | 15 | 15 | 15 | 15 | 15 | 16 | 16 |
| 16 | 16 | 16 | 16 | 16 | 16 | 16 | 16 | 16 | 16 | 16 | 16 | 16 | 16 | 16 | 16 |
| 16 | 16 | 16 | 16 | 16 | 16 | 16 | 16 | 16 | 16 | 16 | 16 | 16 | 16 | 16 | 16 |

The vector D gives the number of daughter particles produced from larger particles in each size class. The first three entries of D are zeros since particles from size classes 1 – 3 are assumed not to be fragmented by krill. For example, a particle from size class 4 produces an average of 2 daughter particles after being fragmented by krill.

$D =$

| | | | | | | | | | | | | | | | |
|---|---|---|------|------|------|------|------|------|------|-------|-------|-------|-------|-------|---|
| 0 | 0 | 0 | 2.00 | 2.30 | 2.60 | 3.50 | 4.10 | 5.70 | 6.50 | 11.80 | 11.50 | 15.30 | 13.80 | 18.30 | 0 |
|---|---|---|------|------|------|------|------|------|------|-------|-------|-------|-------|-------|---|

The matrix ϵ represents a fraction of daughter particles produced from larger particles in each size class. For example, the $(4, 2)^{th}$ provides the proportion of daughter particles of size class 2 produced from fragmenting the particle of size class 4.

$\epsilon =$

| | | | | | | | | | | | | | | | |
|---|------|------|------|------|------|------|------|------|------|------|------|------|------|------|---|
| 0 | 0 | 0 | 0 | 0 | 0 | 0 | 0 | 0 | 0 | 0 | 0 | 0 | 0 | 0 | 0 |
| 0 | 0 | 0 | 0 | 0 | 0 | 0 | 0 | 0 | 0 | 0 | 0 | 0 | 0 | 0 | 0 |
| 0 | 0 | 0 | 0 | 0 | 0 | 0 | 0 | 0 | 0 | 0 | 0 | 0 | 0 | 0 | 0 |
| 0 | 0.74 | 0.09 | 0.17 | 0 | 0 | 0 | 0 | 0 | 0 | 0 | 0 | 0 | 0 | 0 | 0 |
| 0 | 0.30 | 0.15 | 0.35 | 0.20 | 0 | 0 | 0 | 0 | 0 | 0 | 0 | 0 | 0 | 0 | 0 |
| 0 | 0.30 | 0.11 | 0.26 | 0.24 | 0.09 | 0 | 0 | 0 | 0 | 0 | 0 | 0 | 0 | 0 | 0 |
| 0 | 0.26 | 0.07 | 0.20 | 0.23 | 0.18 | 0.06 | 0 | 0 | 0 | 0 | 0 | 0 | 0 | 0 | 0 |
| 0 | 0.23 | 0.11 | 0.13 | 0.22 | 0.14 | 0.11 | 0.05 | 0 | 0 | 0 | 0 | 0 | 0 | 0 | 0 |
| 0 | 0.20 | 0.11 | 0.12 | 0.19 | 0.15 | 0.11 | 0.08 | 0.04 | 0 | 0 | 0 | 0 | 0 | 0 | 0 |
| 0 | 0.11 | 0.06 | 0.10 | 0.15 | 0.11 | 0.08 | 0.08 | 0.04 | 0.26 | 0 | 0 | 0 | 0 | 0 | 0 |
| 0 | 0.13 | 0.06 | 0.08 | 0.17 | 0.11 | 0.09 | 0.05 | 0.04 | 0.25 | 0.01 | 0 | 0 | 0 | 0 | 0 |
| 0 | 0.09 | 0.04 | 0.09 | 0.12 | 0.11 | 0.10 | 0.07 | 0.04 | 0.29 | 0.02 | 0.02 | 0 | 0 | 0 | 0 |
| 0 | 0.13 | 0.07 | 0.06 | 0.15 | 0.11 | 0.10 | 0.04 | 0.04 | 0.24 | 0.03 | 0.02 | 0.01 | 0 | 0 | 0 |
| 0 | 0.10 | 0.06 | 0.08 | 0.11 | 0.10 | 0.09 | 0.06 | 0.05 | 0.26 | 0.03 | 0.02 | 0.02 | 0.02 | 0 | 0 |
| 0 | 0.27 | 0.11 | 0.09 | 0.14 | 0.06 | 0.05 | 0.03 | 0.02 | 0.14 | 0.01 | 0.01 | 0.01 | 0.01 | 0.04 | 0 |
| 0 | 0 | 0 | 0 | 0 | 0 | 0 | 0 | 0 | 0 | 0 | 0 | 0 | 0 | 0 | 0 |

The element of w represents the settling rate of a particle. For example, the settling rate of a particle from size class 1 is $w_1 = 0.0111$ cm per second.

$w =$

Columns 1 through 11

0.0111 0.0209 0.0244 0.0320 0.0433 0.0567 0.0743 0.0971 0.1272 0.1668 0.2186

Columns 12 through 16

0.2865 0.3754 0.4919 0.6445 0.6859

The element of σ refers to the proportion of resulting particles that go to the T_{ij}^{min} class which is equal to class i after the collision between particles of size class i and j with $i \geq j$.

$\sigma =$

Columns 1 through 11

| | | | | | | | | | | |
|--------|--------|--------|--------|--------|--------|--------|--------|--------|--------|--------|
| 0.5000 | 0.5000 | 0.7500 | 0.8750 | 0.9375 | 0.9687 | 0.9844 | 0.9922 | 0.9961 | 0.9980 | 0.9990 |
| 0.5000 | 0.0000 | 0.2500 | 0.6250 | 0.8125 | 0.9063 | 0.9531 | 0.9766 | 0.9883 | 0.9941 | 0.9971 |
| 0.7500 | 0.2500 | 0.0000 | 0.2500 | 0.6250 | 0.8125 | 0.9063 | 0.9531 | 0.9766 | 0.9883 | 0.9941 |
| 0.8750 | 0.6250 | 0.2500 | 0.0000 | 0.2500 | 0.6250 | 0.8125 | 0.9062 | 0.9531 | 0.9766 | 0.9883 |
| 0.9375 | 0.8125 | 0.6250 | 0.2500 | 0.0000 | 0.2500 | 0.6250 | 0.8125 | 0.9063 | 0.9531 | 0.9766 |
| 0.9688 | 0.9062 | 0.8125 | 0.6250 | 0.2500 | 0.0000 | 0.2500 | 0.6250 | 0.8125 | 0.9062 | 0.9531 |
| 0.9844 | 0.9531 | 0.9062 | 0.8125 | 0.6250 | 0.2500 | 0.0000 | 0.2500 | 0.6250 | 0.8125 | 0.9062 |
| 0.9922 | 0.9766 | 0.9531 | 0.9063 | 0.8125 | 0.6250 | 0.2500 | 0.0000 | 0.2500 | 0.6250 | 0.8125 |
| 0.9961 | 0.9883 | 0.9766 | 0.9531 | 0.9063 | 0.8125 | 0.6250 | 0.2500 | 0.0000 | 0.2500 | 0.6250 |
| 0.9980 | 0.9941 | 0.9883 | 0.9766 | 0.9531 | 0.9063 | 0.8125 | 0.6250 | 0.2500 | 0.0000 | 0.2500 |
| 0.9990 | 0.9971 | 0.9941 | 0.9883 | 0.9766 | 0.9531 | 0.9062 | 0.8125 | 0.6250 | 0.2500 | 0.0000 |
| 0.9995 | 0.9985 | 0.9971 | 0.9941 | 0.9883 | 0.9766 | 0.9531 | 0.9062 | 0.8125 | 0.6250 | 0.2500 |
| 0.9998 | 0.9993 | 0.9985 | 0.9971 | 0.9941 | 0.9883 | 0.9766 | 0.9531 | 0.9062 | 0.8125 | 0.6250 |
| 0.9999 | 0.9996 | 0.9993 | 0.9985 | 0.9971 | 0.9941 | 0.9883 | 0.9766 | 0.9531 | 0.9062 | 0.8125 |
| 0.9999 | 0.9998 | 0.9996 | 0.9993 | 0.9985 | 0.9971 | 0.9941 | 0.9883 | 0.9766 | 0.9531 | 0.9063 |
| 1.0000 | 0.9999 | 0.9998 | 0.9996 | 0.9993 | 0.9985 | 0.9971 | 0.9941 | 0.9883 | 0.9766 | 0.9531 |

Columns 12 through 16

| | | | | |
|--------|--------|--------|--------|--------|
| 0.9995 | 0.9998 | 0.9999 | 0.9999 | 1.0000 |
| 0.9985 | 0.9993 | 0.9996 | 0.9998 | 0.9999 |
| 0.9971 | 0.9985 | 0.9993 | 0.9996 | 0.9998 |
| 0.9941 | 0.9971 | 0.9985 | 0.9993 | 0.9996 |
| 0.9883 | 0.9941 | 0.9971 | 0.9985 | 0.9993 |
| 0.9766 | 0.9883 | 0.9941 | 0.9971 | 0.9985 |
| 0.9531 | 0.9766 | 0.9883 | 0.9941 | 0.9971 |
| 0.9062 | 0.9531 | 0.9766 | 0.9883 | 0.9941 |
| 0.8125 | 0.9062 | 0.9531 | 0.9766 | 0.9883 |
| 0.6250 | 0.8125 | 0.9062 | 0.9531 | 0.9766 |
| 0.2500 | 0.6250 | 0.8125 | 0.9062 | 0.9531 |
| 0.0000 | 0.2500 | 0.6250 | 0.8125 | 0.9063 |
| 0.2500 | 0.0000 | 0.2500 | 0.6250 | 0.8125 |
| 0.6250 | 0.2500 | 0.0000 | 0.2500 | 0.6250 |
| 0.8125 | 0.6250 | 0.2500 | 0.0000 | 0.2500 |
| 0.9063 | 0.8125 | 0.6250 | 0.2500 | 0.0000 |